Heating of Tissue by Near-Field Exposure to a Dipole: A Model Analysis

Pere J. Riu, *Senior Member, IEEE*, and Kenneth R. Foster,* *Fellow, IEEE*

***Abstract*—We report a numerical study of the induced electric fields and specific absorption rate (SAR) produced by microwave radiation from a half-wavelength dipole near tissue models, and the resulting transient and steady-state temperature rises. Several models were explored, including a uniform semi-infinite plane of tissue, uniform sphere, a phantom model of the head filled with tissue-equivalent material, a numerical model of the head with uniform dielectric properties (obtained from a digitized computed tomography image), and a numerical model of the head with different dielectric properties corresponding to various tissues. The electromagnetic calculations were performed for half-wave dipoles radiating at 900 and 1900 MHz at various distances from the model, using the finite-difference-time-domain (FDTD) method. The resulting temperature rises were estimated by finite element solution of the bioheat equation. The calculated SAR values agree well with an empirical correlation due to Kuster. If the limiting hazard of such exposures is associated with excessive temperature increase, present exposure limits are very conservative and guidelines that are easier to implement might provide adequate protection.**

***Index Terms*—Bioheat equation, finite difference time domain (FDTD) method, phantom tissue, specific absorption rate (SAR), wireless transmitter.**

I. Introduction

MUCH work has been reported on determining the specific absorption rate (SAR) in the human body (usually, the head) from near-field exposure to a dipole antenna. These studies, using either numerical [1], [2] or experimental methods [3]–[6] were motivated in large part by safety and health concerns about wireless handsets.

The difficulty of this problem is twofold. The SAR cannot be directly measured in the body of a user, but has to be found indirectly by numerical or experimental techniques, both of which are technically difficult and subject to error. Second, the SAR produced in the head by some commercial wireless handsets can approach or marginally exceed limits set by nongovernment bodies (ANSI C95.1-1992 [7], and NCRP [8]), U.S. government agencies (e.g., Federal Communications Commission [9]) as well as European standards [10]. This creates the need for high accuracy in dosimetric studies to verify compliance. We consider a related issue: the possible thermal consequences of such exposure and their implications for the threshold for hazard.

Manuscript received July 23, 1998; revised January 5, 1999. This work was supported in part by a personal grant to P. J. Riu from the Dirección General de Investigación Científica y Técnica of the Spanish Government, by Lucent Technologies, Inc., and by the University of Pennsylvania Research Foundation. *Asterisk indicates corresponding author.*

P. J. Riu is with the Departament d'Enginyeria Electronica, Universitat Politecnica de Catalunya, Barcelona, Spain.

*K. R. Foster is with the Department of Bioengineering, University of Pennsylvania, 220 S. 33rd St., Philadelphia, PA 19104-8534 USA (e-mail: kfoster@eniac.seas.upenn.edu).

Publisher Item Identifier S 0018-9294(99)05766-3.

II. Methods

The SAR was determined numerically in a range of tissue models from near-field exposure to a half-wave dipole at 900 or 1900 MHz. The models included a semi-infinite plane, a uniform sphere modeling the human head, a numerically digitized image of a phantom head model (Schmid and Partner Engineering AG, Zurich, Switzerland) and a numerical model of the human head from an magnetic resonance imaging scan (Remcom, Inc., State College, PA). The models are summarized in Tables I and II.

In each of these models, the induced SAR was calculated using a commercial finite difference time domain (FDTD) program, XFDTD (Remcom, Inc., State College PA) on a Sun Ultra 1 workstation. The digitized image of the head phantom was produced by filling the model with water, scanning it with computed tomography (CT) in the Department of Radiology of the University of Pennsylvania, Philadelphia, and thresholding the image to produce a three-level image representing air, the polymer shell of the model, and the liquid within it. The FDTD calculations were done with a grid spacing of 3 mm, except for calculations using the CT image of the head phantom, which were done with a resolution of 2 mm. The calculations were repeated with the dipoles at various distances from the models.

Most of the calculations on the simplified models were performed with the same set of dielectric parameters ($\epsilon_r = 80$, $\sigma = 1$ S/m). Those with the dielectrically realistic model of the head (Remcom) were performed with the values listed in Table II. The same values for the dielectric properties of the tissues were used at the two frequencies of simulation. In reality, the conductivity of soft tissues increases with frequency, but reported values for soft tissues are in the range 1–2 S/m at both frequencies [11]. The major conclusions of this study would not change if somewhat different values for the dielectric properties of tissues were employed.

The dipoles were excited at the center feedpoint, and the transmitted power was determined from the complex product of current and voltage at the feedpoint. The results were normalized to a transmitted power of 600 mW (900 MHz) or 125 mW (1900 MHz), the approximate maximum output

TABLE I
MODELS STUDIED

Model	Dielectric Properties	Comments
1. Uniform semi-infinite plane	$\sigma = 1$ S/m $\epsilon_r = 80$	Dipole parallel to plane
2. Uniform sphere	$\sigma = 1$ S/m $\epsilon_r = 80$	Dipole perpendicular to radius of sphere
3. Head phantom	$\sigma = 0.86$ S/m $\epsilon_r = 52$	Obtained by CT scan of a model obtained from Kuster (Zurich, Switzerland) dipole parallel to right side of head
4. Uniform head model	$\sigma = 1$ S/m $\epsilon_r = 80$	Obtained by CT scan of human head (from Remcom, Inc.) Dipole parallel to side of head.
5. Realistic head model	See Table 2	Same as above, with dielectric properties of head tissues summarized in Table 2. Dipole parallel to side of head.

TABLE II
DIELECTRIC PROPERTIES OF TISSUES ASSUMED IN REMCOM HEAD MODEL

Tissue	Permittivity (900, 1900 MHz)	Conductivity (900, 1900 MHz)
Fat, bone	5.1	0.07 S/m
Muscle	52.6	1 S/m
Nerve, brain	44	0.75 S/m
Eye	70	1.9 S/m
Blood	62	1.18 S/m
Cartilage	5.1	0.07 S/m
Skin	52.6	1 S/m

of commercial cellular and personal communications services (PCS) handsets.

In the plane tissue model, the resulting temperature rise was calculated with a two-dimensional (2-D) finite element model (PDEase, Macsyma Inc. Arlington MA). The SAR patterns were obtained from the FDTD calculations, in a plane perpendicular to the dipole passing through its feedpoint. These data were used as input to the bioheat equation: where

$$k\nabla^2 T - \rho_b \rho_t C_b m_b T + \rho_t \mathrm{SAR} = C_t \rho_t \frac{dT}{dt} \qquad (1)$$

where

- T temperature of the tissue (°C) above mean arterial temperature;
- k thermal conductivity of tissue (0.6 W/m · °C);
- SAR microwave energy deposition rate (W/kg);
- C_b heat capacity of blood (4000 W ∗ s/kg · °C);
- C_t heat capacity of tissue (4000 W ∗ s/kg · °C);
- ρ_b density of blood (1000 kg/m^3);
- ρ_t density of tissue (1000 kg/m^3);
- m_b volumetric perfusion rate of blood ("normal" blood perfusion was taken to be 40 cm^3/100 g ∗ min).

In the discussion below we assume for simplicity that $\rho_b = \rho_t = \rho$ and $C_b = C_t = C_p$. Calculations were done with adiabatic boundary conditions at the surface, i.e., no heat loss from the plane into space. The simplified 2-D heat flow calculations are justified because the spatial gradients of the SAR patterns beneath the antenna feedpoint are much larger in a direction perpendicular rather than parallel to the dipole. Thus, heat conduction will be primarily in the plane in which the heat flow calculations were performed.

III. RESULTS

A. SAR Contours

Fig. 1 shows the SAR contours (1900 MHz) in the tissue plane, for several distances between the dipole and the plane, in planes parallel and perpendicular to the dipole. The largest electric field component in the tissue is directed parallel to the dipole, and occurs at the surface directly beneath the feedpoint of the antenna, in agreement with earlier reports, e.g., [5]. This field component arises from the currents induced by the magnetic fields from the dipole. Fig. 2 shows the SAR at the surface of the plane, at several distances from the feedpoint as a function of the distance from the dipole to the plane.

B. Energy Penetration Depth

Fig. 3 shows the SAR in the different models, along a radius extending into the model, perpendicular to the dipole and centered beneath the feedpoint, at 900 MHz and 1.9 GHz for the dipole placed 9 mm from the surface. The pattern and depth of energy penetration depend strongly on the distance from the dipole to the tissue, but less strongly on the geometry of the model. In all the cases the penetration depth is smaller than that for plane waves of the same frequency. The penetration depth also depends on the distance from the dipole to the plane, decreasing markedly when the dipole is brought close to the

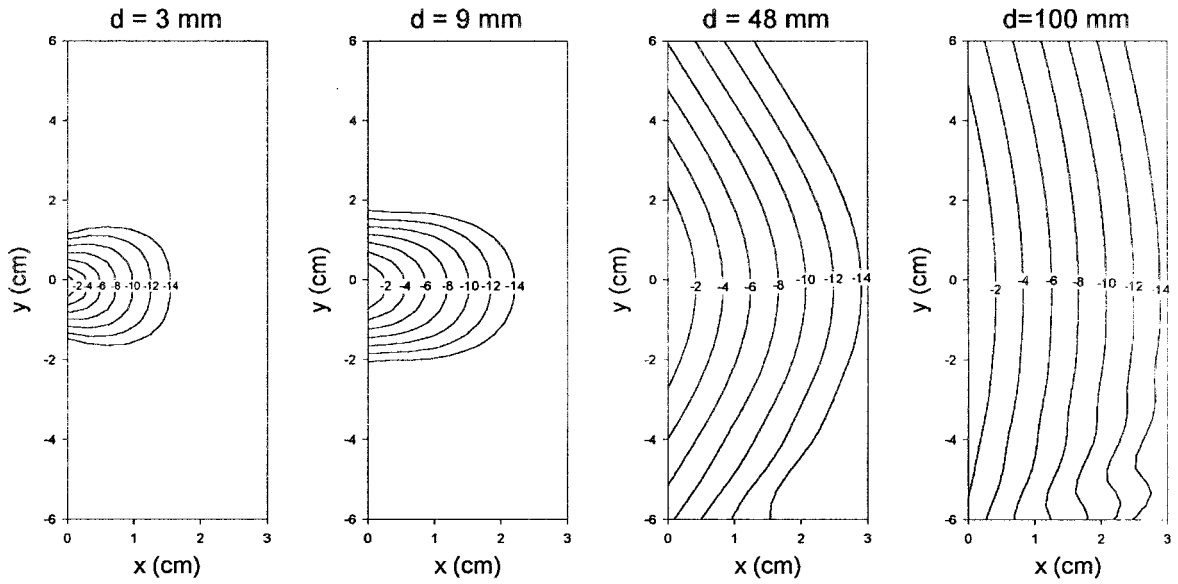

(a)

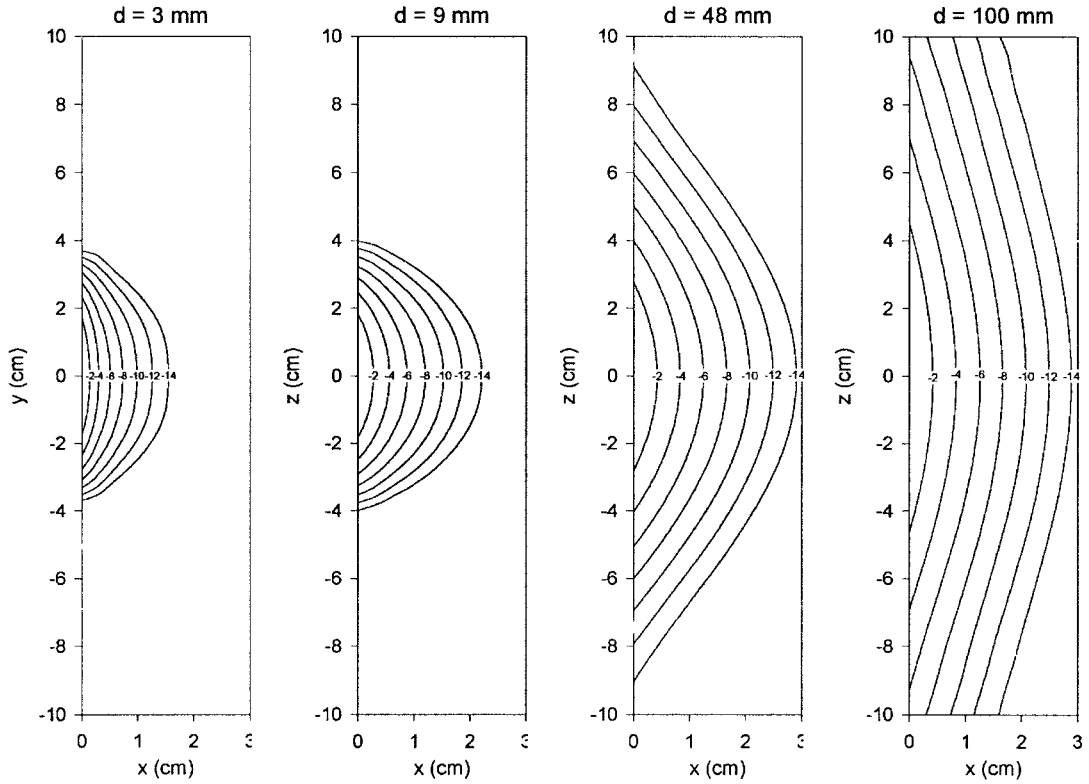

(b)

Fig. 1. Contours for SAR in tissue plane beneath the 1900-MHz dipole at different distances d of the dipole from the plane. (a) Contours in a plane perpendicular to the dipole, passing through the feedpoint. (b) Contours in the plane containing the dipole, normal to the tissue surface. SAR is in dB normalized to the maximum value. Contour lines at -2-dB increments.

surface. In all cases examined, most of the energy is absorbed in the reactive (near field) region of the dipole.

C. Thermal Response

Fig. 4 shows the transient temperature rise in the plane model, for dipoles at 900 and 1900 MHz. The results were normalized to a radiated power of 0.6 W (900 MHz) or 0.125 W (1900 MHz). Also shown is the sensitivity parameter S

$$S = \frac{m_b}{T}\frac{\partial T}{\partial m_b}. \tag{2}$$

This parameter is interpreted simply as the percent of change in temperature per percent change in blood flow. This is significant in the present context because the blood flow is uncertain, [and (1) is at best a very approximate description

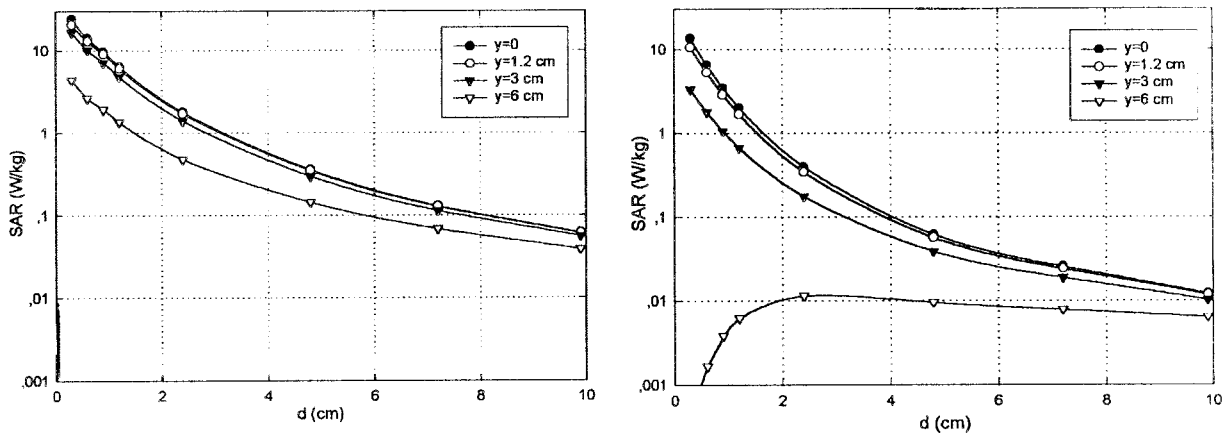

(a) (b)

Fig. 2. The SAR at the surface of the tissue plane at several distances y from the feedpoint, as a function of the distance from the dipole to the plane: (a) 900 and (b) 1900 MHz.

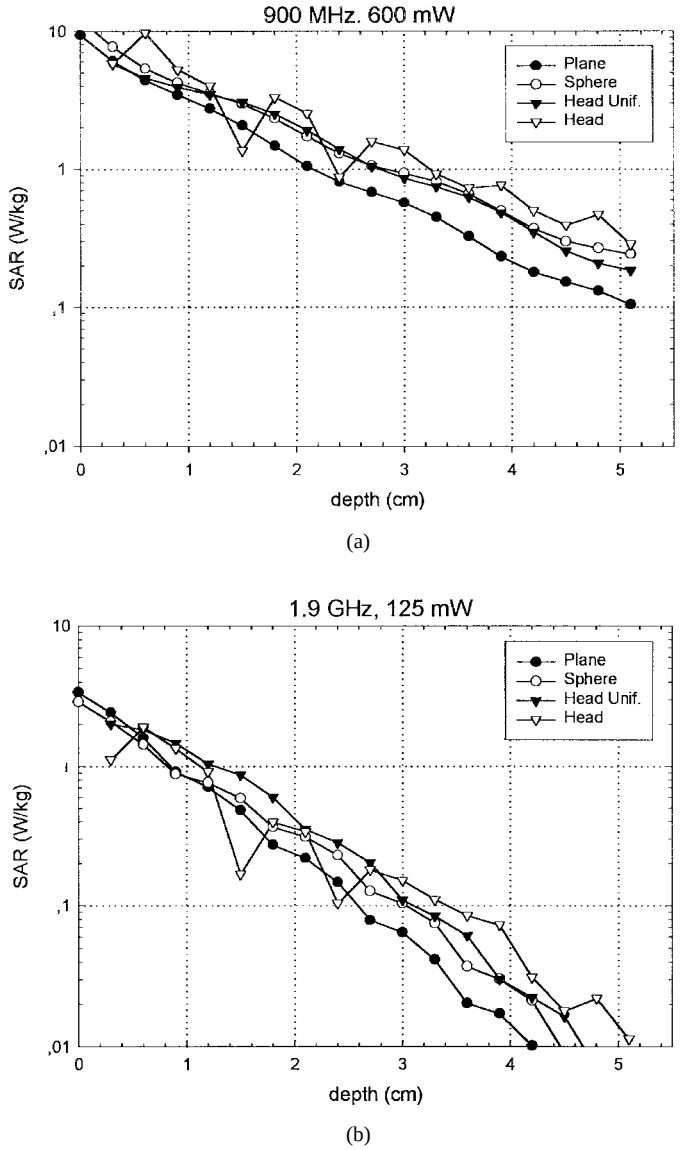

(a)

(b)

Fig. 3. SAR directly beneath the feedpoint of the dipole versus depth into the model, for several models listed in Table I. The variability in the SAR in the nonuniform head model arises from different tissue types: skin, muscle, skull, and brain.

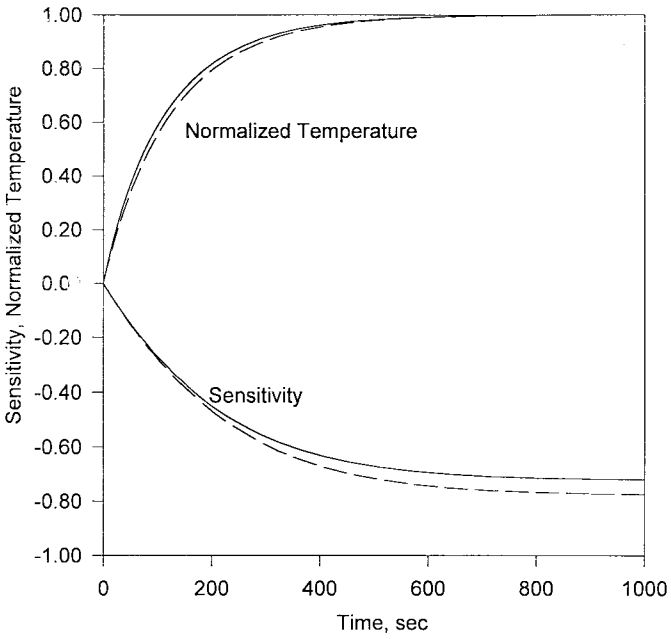

Fig. 4. Transient temperature rise at the surface of the plane beneath the feedpoint of the dipole versus time for normal blood flow (40 cm^3/100 g min). The radiated power was 0.6 W (900 MHz) (dashed line) or 0.125 W (1900 MHz) (solid line). Also shown are the corresponding sensitivity of the temperature with respect to the blood flow parameter. The temperatures have been normalized by the steady-state values 0.045 °C (0.9 GHz) and 0.033 °C (1.9 GHz). Both dipoles are 2.4 cm above plane.

of convective cooling by blood], whereas thermal conduction is a well characterized process.

The sensitivity is small in the transient period of heating but approaches -0.7 to -0.8 as the steady-state is reached. This indicates that the temperature rise for the first minute or so of heating is hardly affected by the blood flow (there is insufficient time for significant heat transfer to take place). In the steady-state, the temperature rise is (nearly) inversely proportional to the blood flow.

Fig. 5 shows the maximum steady-state temperature rise in the tissue plane produced by a dipole radiating 0.6 W at 900 MHz, versus blood perfusion rate m_b, calculated using the 2-D

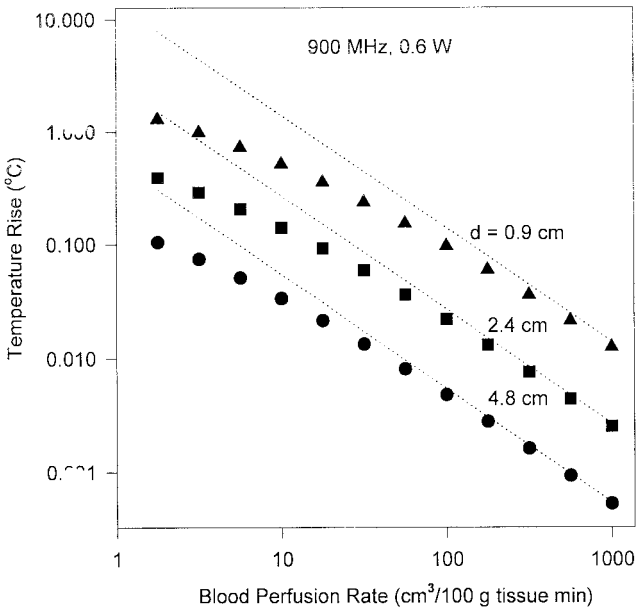

Fig. 5. Maximum steady-state temperature rise in tissue plane a dipole radiating 0.6 W at 900 MHz versus blood perfusion parameter m_b. Distances of the dipole above the plane are indicated on the figure. Physiologically reasonable perfusion rates are in the range 10–100 cm^3/100-g min. The dotted lines show the limiting temperature rise from (9).

finite element routine. The results agree well with (9), which predicts the steady-state temperature rise in the absence of heat conduction (i.e., for convection-limited heat transfer).

IV. Discussion

A. Comparison of Numerical and Analytical Approximations to SAR

Kuster and Balzano [5] have reported an approximate result for $\mathrm{SAR}_{\max}$, the maximum SAR at the surface of a plane from a nearby dipole

$$\mathrm{SAR}_{\max} = \frac{\sigma}{\rho}\frac{\mu\omega}{\sqrt{\sigma^2+\varepsilon^2\omega^2}}(1+C_{\mathrm{corr}}\gamma_{\mathrm{pw}})^2\frac{I_{\mathrm{fp}}^2}{(2\pi d)^2} \tag{3}$$

where

$$\begin{aligned} C_{\mathrm{corr}} &= 1, \quad d \geq 0.08\lambda/\gamma_{\mathrm{pw}} \\ &= \sin\left(\frac{\pi}{2}\frac{Y_{\mathrm{pw}}}{0.08}\frac{d}{\lambda}\right), \quad d < 0.08\lambda/\gamma_{\mathrm{pw}} \end{aligned} \tag{4}$$

is an empirical correction factor that takes into account the presence of the plane on the radiated power from the antenna.

d	Distance from the dipole to the plane.
γ_{pw}	Plane-wave reflection coefficient for the field.
λ	Free space wavelength.
ρ	Mass density of the material.
(μ,ϵ,σ)	Permeability, permittivity, and conductivity of the material.
I_{fp}	Antenna current at the feed point.

TABLE III
FDTD Versus Numerical Approximations, Dipole Above Uniform Plane

Distance of dipole from plane, cm	RMS current at feedpoint, mA	Input impedance, (determined by FDTD), ohm	Maximum SAR, FDTD, W/kg	Maximum SAR, Eq (3), W/kg
0.3	36.2	96+j7.7	10.9	15.1
0.6	41.6	71-j0.6	5.8	5.1
0.9	43.2	66-j12.3	3.2	2.8
1.2	41.3	67-j21.7	1.9	1.6
2.4	37.8	87-j43	0.39	0.40
4.8	29.8	129-j24.3	0.056	.056
7.2	33.0	114-j4.1	0.026	.030
9.9	33.9	104	0.012	.017

(1900 MHz, 7.5 cm. dipole radiating 0.125 W; ϵ=80; σ = 1 S/m)

This approximation was obtained in [5] by fitting the results of many calculations of SAR in a tissue plane from an electric dipole in the near field. Our present results, which are based on similar calculations, are in close agreement, except at the shortest distance where the disagreement may result from finite grid size effects in the present calculations (see Table III).

King [12], [13] reported an approximate analysis for the SAR induced in a two-layer plane from the near field of a $\lambda/2$ dipole. King's analysis considered an "effective dipole" whose length is 60% that of a half-wave dipole, excited with a uniform current distribution. This simplified model yields analytical (but complicated) expressions for the induced fields and SAR. Our results are in reasonable agreement with those results. However, precise comparisons are not possible because the theory does not account for changes in the antenna impedance in very near-field exposures [which are accounted for in (4)], which influence the radiated power.

B. Temperature Rise

The thermal response can be clarified by writing (1) using dimensionless quantities (x',t',T')

$$\begin{aligned} T &= \frac{Tk}{\rho \mathrm{SAR}_o L^2} = \frac{T}{\tau_2}\frac{C_p}{\mathrm{SAR}_o} \\ x' &= \frac{x}{L} \\ t' &= \frac{tk}{\rho C_p L^2} = t/\tau_2 \\ \mathrm{SAR}' &= \frac{\mathrm{SAR}}{\mathrm{SAR}_o} \end{aligned} \tag{5}$$

where L is a characteristic distance scale of the heating and SAR_o characterizes the exposure (normally, the maximum SAR in the heated volume). The time constants τ_1 and τ_2 are

$$\begin{aligned} \tau_1 &= \frac{1}{\rho_b m_b} \\ \tau_2 &= \frac{\rho C_p L^2}{k}. \end{aligned} \tag{6}$$

Equation (1) then becomes

$$\nabla^2 T' - \frac{\tau_2}{\tau_1}T' + \mathrm{SAR}'(x',t) = \frac{\partial T'}{\partial t'}. \tag{7}$$

The first time constant, τ_1, is associated with thermal convection, and is 150 s for the normal value for blood flow given above. The second time constant, τ_2, is associated with heat conduction, and is about 1000 s for plane waves incident on soft tissue at 1 GHz. Thus $\tau_2 > \tau_1$ under the exposure conditions considered here. In the limiting case where thermal gradients are small $(\nabla^2 T' < 1)$, (7) simplifies to

$$\mathrm{SAR}'(x',t) - \frac{\tau_2}{\tau_1} T' \approx \frac{\partial T'}{\partial t'} \tag{8}$$

which has the steady-state solution (for time-independent SAR), in dimensioned units

$$T(x,\infty) = \frac{\mathrm{SAR}(x)}{\rho C_p m_b}. \tag{9}$$

In this limit, the steady-state temperature rise is simply proportional to the SAR and the temperature approaches its steady-state as a simple exponential process. The sensitivity S then is -1. Similar considerations for the one-dimensional case (a semiinfinite plane of tissue exposed to plane wave energy) results in sensitivity of -1 for convection limited heating $(\tau_2 > \tau_1)$ and $-1/2$ for conduction limited heating $(\tau_2 < \tau_1)$ [14].

The numerical results are in close agreement with this approximation, at both frequencies of simulation, for physiologically reasonable blood flow rates. Thus, contours of the steady-state temperature rise beneath the dipoles closely resemble the SAR contours, and are not shown.

C. Comments on Exposure Standards

From (3) it is clear that even low-powered sources can produce significant SAR's if located sufficiently close to the tissue. We consider the thermal consequences of such exposure with respect to RF exposure standards, in particular ANSI/IEEE C95.1-1992; similar comments would apply to other major standards as well.

ANSI/IEEE C95.1-1992 has two relevant provisions. The first is a limit on partial body exposure, to 1.6 or 8 W/kg (uncontrolled or controlled exposure) averaged over any gram of tissue. From (9), this corresponds to a steady-state temperature rise of 0.06 °C or 0.3 °C (for normal blood flow).

The second is a "low power exclusion" in ANSI/IEEE C95.1 (but not in various government limits) that removes the need to determine SAR for low-power sources between 0.45 and 1.5 GHz located more than 2.5 cm from the body. The exclusion for controlled environments is

$$P = 7\left(\frac{0.45}{f_{\mathrm{GHz}}}\right)\text{watts} \tag{10}$$

where f_{GHz} is the frequency in GHz; that for uncontrolled environments is a factor of five smaller. For controlled environments. (3), (4), (9), and (10) lead to maximum steady-state temperature rises of about 1 °C, with corresponding values for uncontrolled environments a factor of five smaller. In both cases, the steady-state temperature is approached after several minutes of exposure. Fig. 6 shows the calculated temperature rise (from numerical solutions of the bioheat equation) for several distances and assumed blood flow parameters.

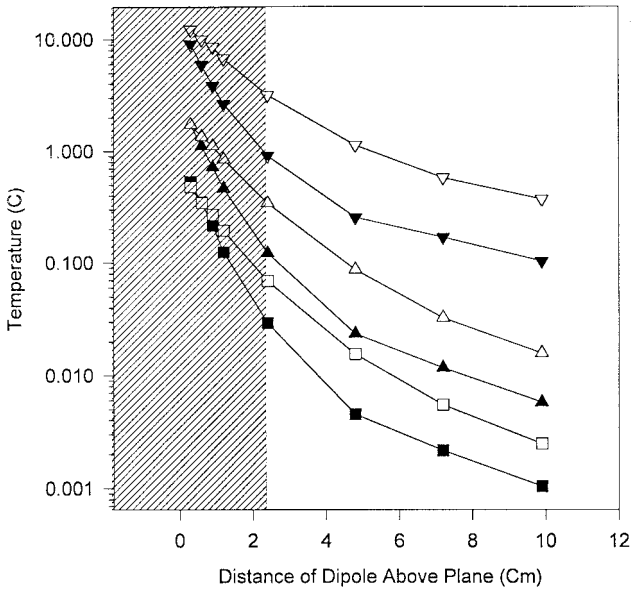

Fig. 6. Maximum temperature rise in tissue plane as a function of the distance of the dipole above it. The results are for half-wave dipoles radiating 0.350 W (1900 MHz; solid symbols) or 0.7 W (900 MHz; open symbols) Blood flow parameters are normal blood flow (squares), $1/10$ normal blood flow, (triangles) or no blood flow (inverted triangles). The shaded area represents distances <2.5 cm, the minimum distance from the antenna to the plane required by the ANSI/IEEE C95-1992 exclusion.

How "safe" the limits are depends on the hazards the standard is designed to protect against. The major RF exposure standards were developed by identifying the adverse effect of RF exposure that was reliably reported in animals at the lowest SAR. In ANSI/IEEE C95.1-1992 and other major standards, this limiting hazard is "behavioral disruption," as reported in several species at whole-body SAR's of about 4 W/kg. Behavioral disruption occurs when an animal stops performing a task (e.g., pressing a lever) and begins a different behavior (e.g., spreading saliva on the tail, which is a thermoregulatory response in rats), and is clearly a result of excessive body heating.

With behavioral disruption as the critical effect, ANSI/IEEE C95.1-1992 was designed to limit whole body exposure to 0.08 or 0.4 W/kg for uncontrolled or controlled environments (which correspond roughly to general public and occupational exposures). Thus, the standard has a safety factor in excess of 10 or 50, for controlled or uncontrolled environments, for whole body exposures.

The limits for partial body exposure are based on the observation that in whole body exposure to plane waves, the ratio of the maximum to whole-body average SAR is about 20:1 [15]. Thus the limits in ANSI/IEEE C95.1-1992 for partial body exposure are 1.6 or 8 W/kg, i.e., 20 times higher than for whole body exposure. This rationale is, at best, unclear.

For partial body exposure, the limiting hazard may be local temperature rise, rather than excessive thermal load to the body. Thermal injury is characterized by a rate process, such that the threshold for injury depends on the duration and

magnitude of temperature rise (more precisely, the thermal dose). However, for extended heating periods (minutes) the threshold temperature rise for tissue damage is about 10 °C.

By this measure, the "low power exclusion" in ANSI/IEEE C95.1-1992 represent a safety factor of about 10–50, about the same as the limits for whole body exposure. The safety factors based on the limits of 1.6 or 8 W/kg are much higher, ranging from 35 (controlled) to 170 (uncontrolled environment), based on steady-state heating with normal blood flow.

The required size of the safety factor is a normative issue with practical consequence in the regulatory arena and elsewhere. In particular, the margin of safety affects the accuracy that should be required for verifying compliance. If the limiting hazards are thermal, the standards are clearly very conservative. Under these conditions, the demand for very accurate studies to verify compliance creates difficult engineering problems that have no likely benefit for health and safety. Several different electromagnetic models all lead to the same general results for power deposition (Fig. 3) so the choice of model is not critical.

This discussion does not imply that only thermal hazards exist ("nonthermal" hazards are beyond the scope of the present paper). If other hazards exist, the whole basis for the standards would have to be reexamined in any event.

ACKNOWLEDGMENT

The authors would like to thank the anonymous referees for several important suggestions.

REFERENCES

[1] O. P. Gandhi, G. Lazzi, and C. M. Furse, "Electromagnetic absorption in the human head and neck for mobile telephones at 835 and 1900 MHz," *IEEE Trans. Microwave Theory Tech.*, vol. 44, pp. 1884–1897, 1996.

[2] S. Gutschling and T. Weiland, "Detailed SAR distributions in high resolution human head models,"

[3] R. F. Cleveland Jr. and T. W. Athey, "Specific absorption rate in models of the human head exposed to hand-held UHF portable radios," *Bioelectromagn.*, vol. 10, pp. 173–186, 1989.

[4] V. Anderson and K. H. Joyner, "Specific absorption rate levels measured in a phantom head exposed to radio frequency transmissions from analog hand-held mobile phones," *Bioelectromagn.*, vol. 16, pp. 60–69, 1995.

[5] N. Kuster and Q. Balzano, "Energy absorption mechanism by biological bodies in the near field of dipole antennas above 300 MHz," *IEEE Trans. Veh. Tech.*, vol. 41, pp. 17–23, 1992.

[6] N. C. Skaropoulos, M. P. Ioannidou, and D. P. Chrissoulidis, "Induced em field in a layered eccentric spheres model of the head: Plane-wave and localized source exposure," *IEEE Trans. Microwave Theory Tech.*, vol. 44, pp. 1963–1973, 1996.

[7] "Safety Levels with Respect to Human Exposure to Radiofrequency Electromagnetic Fields, 3 kHz to 300 GHz," ANSI/IEEE Standard C95.1-1992,

[8] National Council on Radiation Protection and Measurements, "Biological effects and exposure criteria for radiofrequency electromagnetic fields," NCRP, Bethesda, MD., Tech. Rep. 861986.

[9] U.S. Federal Communications Commission, In the matter of guidelines for evaluating the environmental effects of radiofrequency radiation, Docket no. 93-62, Aug. 1, 1996.

[10] Human Exposure to Electromagnetic Fields, High Frequency (10 kHz to 300 GHz), Standard CEN/CENELEC ENV 50166-2:1995.

[11] K. R. Foster and H. P. Schwan, "Dielectric properties of tissues," in *Handbook of Biological Effects of Electromagnetic Fields*, 2nd ed, C. Polk and E. Postow, Eds. Boca Raton FL: CRC, 1996, pp. 27–106.

[12] R. W. P. King, "The electromagnetic field of a horizontal electric dipole in the presence of a three-layered region," *J. Appl. Phys.*, vol. 69, pp. 7987–7995, 1991.

[13] R. W. P. King, "Electromagnetic field generated in model of human head by simplified telephone transceiver," *Radio Sci.*, vol. 30, pp. 267–281, 1995.

[14] K. R. Foster and L. S. Erdreich, "Thermal models for microwave hazards and their role in standards development," *Bioelectromagn.*, in press.

[15] R. Petersen, personal communication to K. Foster, April 97.

Pere J. Riu (S'86–M'91–SM'98) was born in Gironella, Spain, in 1962. He received the engineering and Ph.D. degrees from the Universitat Politècnica de Catalunya, Barcelona, Spain, in 1986 and 1991, respectively.

Since 1986 he has held different faculty positions at the Universitat Politècnica de Catalunya and currently is Associate Professor in the Department of Electronic Engineering. In 1997, he was visiting associate professor in the Department of Bioengineering, University of Pennsylvania, PA, doing research on the biological effects of RF electromagnetic fields. He is active in research in clinical and industrial applications of electrical bioimpedance, specially in impedance imaging. His research interests also include electromagnetic compatiblity problems applied to automotive systems.

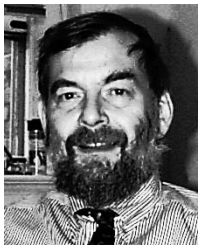

Kenneth R. Foster (M'77–SM'81–F'88) received the Ph.D. degree in 1971.

He is Associate Professor of Bioengineering at the University of Pennsylvania. Since 1971, he has been engaged in studies on the interaction of nonionizing radiation and biological systems, including studies on mechanisms of interaction and biomedical applications of radiofrequency and microwave energy. In addition he has written widely about scientific issues related to possible health effects of electromagnetic fields. He has published approximately 90 technical papers in peer reviewed journals, numerous other articles, and is the author of two books related to technological risk; most recently *Judging Science* (Cambridge, MA: MIT Press, 1997).

Dr. Foster is Chair of the IEEE EMBS Committee of Man and Radiation. In 1997–1998, he served as President of the IEEE Society on Social Implications of Technology.